Research Article Open Access

Yuhan Wei, Lei Xu, Shengjiao He, Chenglei Li, Qi Wu, Xianyin Zeng, Hanguang Wang and Kuan Liu*

Novel benzimidazole-based conjugated polyelectrolytes: synthesis, solution photophysics and fluorescent sensing of metal ions

https://doi.org/10.1515/epoly-2020-0003
Received July 27, 2019; accepted October 08, 2019.

Abstract: Two benzimidazole-based conjugated polyelectrolytes (+)-PPBIPV and (-)-PPBIPV which have opposite charges on their side chains were synthesized via Heck coupling reaction and characterized by ^{1}H-NMR, UV-vis and PL spectroscopy. These two polyelectrolytes are both consisted of benzimidazole derivatives and phenylene-vinylene units. The absorption and emission spectra reveal that the polymers both have solvent-dependency and concentration-dependency, and they exhibit aggregation effect in aqueous solution. In the respect of ion detection, the aqueous solution of (+)-PPBIPV has excellent selectivity and sensitivity for Fe^{3+}. Moreover, Pd^{2+} can almost completely quench the fluorescence of (+)-PPBIPV in methanol solution, and its quenching constant K_{SV} is 5.93×10^4 M^{-1}. For (-)-PPBIPV, Sn^{2+} can double the fluorescence intensity of its aqueous solution, while (-)-PPBIPV has good identification for Fe^{3+} in methanol with a K_{SV} = 3.44×10^5 M^{-1}. Hence, two polyelectrolytes have considerable potential to become effective fluorescent sensing materials for some specific metal ions. All of the stoichiometric relationships between metal ions and conjugated polyelectrolytes were calculated using Benesi-Hildebrand equation.

Keywords: conjugated polyelectrolytes; benzimidazole; fluorescence quenching; Stern-Volmer plot; Benesi-Hildebrand plot

*** Corresponding author: Kuan Liu,** College of Science, Sichuan Agricultural University, Yaan 625014, China, e-mail: cosmicer@live.cn
Yuhan Wei, Lei Xu, Shengjiao He and Hanguang Wang, College of Science, Sichuan Agricultural University, Yaan 625014, China
Chenglei Li, Qi Wu and Xianyin Zeng, College of Life Science, Sichuan Agricultural University, Yaan 625014, China

1 Introduction

Conjugated polyelectrolytes (CPEs) which are a kind of conjugated polymers with water soluble ionic groups have received considerable interests in the past decades. Their ionized side-chain groups make CPEs have excellent solubility in water and other polar solvents. CPEs are a versatile class of materials that have been applied in a variety of photoelectric devices including polymer light-emitting diodes (PLEDs) (1), photovoltaic cells (2) and chemical and biological sensors (3,4). In particular, the chemical structure of CPEs offers several advantages in sensor applications, such as the increasing sensitivity of detection and water solubility. Therefore, CPEs have been widely explored as optical probes for various targets, such as DNA (5), proteins (6), small molecules (7) and metal ions (7,8).

The conjugated polyelectrolytes can be classified into cationic and anionic types depending on the different charged groups introduced on the side chain. Specifically, few cationic conjugated polyelectrolytes were reported and almost all of them were not synthesized directly but prepared by quaternization after the polymerization. Since not all the side groups of the polymers are electrically charged during this process, fully charged cationic polyelectrolytes cannot be obtained by indirect method. In recent years, cationic CPEs have potential applications in biological imaging such as folate receptor (FR) over expressed cancer cells (9), selective recognition of mammalian cells (10) and anionic surfactants (11), monitoring the physical changes of lipid membrane (10). On the other hand, anionic CPEs have been widely applied in the biological and chemical analysis area with their excellent water solubility. Direct electron transfer over a longer working distance can be accomplished through the sulfonated conjugate polyelectrolyte, which has a strong signal in DNA detection (12). And a probe system as fluorescence turn-on assay of simple saccharides is based on three anionic conjugated polyelectrolytes and

three quenched molecules substituted by boric acid (13). However, almost all the anionic CPEs are consisted of phenyl units (14), thiophene derivatives (15) and fluorene monomers (16), and there are few literatures focused on water soluble N-heterocyclic systems. This can be attributed to complexity of the synthesis and purification. Although the fluorescent sensing properties of conjugated polyelectrolytes in the field of biology and chemistry have been extensively studied, there are few reports on the detection of metal ions in both cationic and anionic conjugate polyelectrolytes.

Benzimidazole is a nitrogen-containing heterocyclic compound fused from an imidazole ring and a benzene ring. With chemical modification by using various specific chemical methods, derivatives of benzimidazole can interact with enzymes, receptors and metal ions in the living body (17). Therefore, they have a wide range of applications in medicine (18) and pesticides (19). In recent years, due to the structural characteristics of benzimidazole, its derivatives have also received extensive attention in the field of fluorescent sensors (20). The sp^2 hybridized nitrogen atom on benzimidazole has a lone pair of electrons that can coordinate with metal ions, resulting in changes in optical properties to achieve the purpose of detection (21). Thus, there have been a number of reports about small molecule probes containing benzimidazole (22,23). Related studies on benzimidazole-containing conjugated polymers reported in the past have mainly focused on light-emitting diodes (24) and photovoltaic devices (25). However, few benzimidazole-based conjugated polymers have been utilized for fluorescent sensors, and they are basically oil soluble (26). Among these studies, most of the fluorescence sensing properties were investigated in non-aqueous system, such as tetrahydrofuran (27). Therefore, it is interesting to develop novel CPEs containing benzimidazole which can detect metal ions in the water effectively.

Herein, we have successfully designed and synthesized two novel conjugated polyelectrolytes cationic PPBIPV ((+)-PPBIPV) and anionic PPBPIV ((-)-PPBIPV), which were modified with quaternary ammonium salt and sulfonate in the side-chain, respectively. First, the synthesis and characterization of two monomers 5-bromo-2-(4-bromophenyl)-1-ethyl-1H-benzo[d]imidazole (monomer 1) and 5-bromo-2-(4-bromophenyl) -1-(3-sulfonylpropyl) -1H-benzo[d]imidazole (monomer 2) were accomplished. And then the two compounds were used as the copolymerization monomers to synthesize (+)-PPBIPV and (-)-PPBIPV via Heck coupling reaction with 1,4-Bis(3-(N,N,N-triethylammonium)-1-oxapropyl)-2,5-divinyl-benzene dibromide ((+)-DVB) and 1,4-divinyl-2,5-dibutyloxy-benzene (C4-DVB), respectively. Photophysics properties of (+)-PPBIPV and (-)-PPBIPV were studied with absorption and emission spectra by changing the kind of solvent. In the respect of metal sensing, we used fluorescence spectroscopy to investigate the metal ions response of (+)-PPBIPV and (-)-PPBIPV in aqueous solution and methanol solution, respectively. The fluorescence of these solutions is obviously affected with addition of specific metal ions, and these two polyelectrolytes which are oppositely charged exhibit totally different metal sensing properties, demonstrating their potential as metal ion probes. The results of this study can provide useful suggestions for the design and synthesis of novel conjugated polyelectrolytes materials in the area of fluorescence chemical sensor.

2 Experimental

2.1 Measurements

^{1}H NMR spectra were recorded on a Bruker Avance II-400MHz spectrometer (Bruker, Karlsruhe, Germany) with tetramethylsilane as an internal reference. UV-vis absorption spectra were performed on an AnalytikJena Specord 200Plus UV-vis spectrophotometer (AnalytikJena, Jena, Germany). Photoluminescence (PL) spectra were measured by using a Hitachi F-4600 luminescence spectrophotometer (Hitachi, Tokyo, Japan). All spectra were measured at room temperature.

2.2 Materials

All of chemicals were purchased from Aladdin Industrial Corporation (Aladdin, Shanghai, China) and were used directly without further purification. 1,4-divinyl-2,5-dibutyloxy-benzene (C4-DVB) and 1,4-Bis(3-(N,N,N-triethylammonium)-1-oxapropyl)-2,5-divinyl-benzene dibromide ((+)-DVB) were synthesized according to the literature (28). 4-bromo-2-nitroaniline (1) and 4-bromobenzene-1,2-diamine (2) were prepared following the published procedures (29,30).

2.2.1 Synthesis of monomers

5-Bromo-2-(4-bromophenyl)-1H-benzo[d]imidazole (3)

4-bromobenzaldehyde (1.1 g, 6 mmol), sodium bisulfite (0.6 g, 6 mmol), and absolute ethanol (25 mL) were stirred

at room temperature for 4 h. Then 4-bromobenzene-1,2-diamine(2) (1.1 g, 6 mmol) dissolved in DMF (15 mL) was added. The reaction mixture was subjected to reflux for 2 h. Subsequently, ethanol in the mixture was removed by rotary evaporation. The residue was dissolved in 20 mL ethyl acetate and washed with water. The organic phase was dried over anhydrous sodium sulfate, and then filtered. The solvent was removed by rotary evaporation and the crude product was purified by column chromatography (silica gel, petroleum ether/ethyl acetate: 4/1) to give a white solid. Yield: 1.30 g, 61.5%. ^{1}H NMR (400 MHz, DMSO-d_6, δ): 13.22 (s, 0.5H), 13.18 (s, 0.5H); 8.11 (d, J = 6.9 Hz, 2H); 7.90-7.68 (m, 3H); 7.63 (d, 0.5 H), 7.51 (d, 0.5 H); 7.36 (m, J = 9.4 Hz, 1H).

5-Bromo-2-(4-bromophenyl)-1-ethyl-1H-benzo[d]imidazole (monomer 1)

Under argon atmosphere, 5-bromo-2-(4-bromophenyl)-1H-benzo[d]imidazole(3) (1.5 g, 4 mmol) in DMF (15 mL) was stirred at 0°C and then sodium hydride (60%) (0.56 g, 14 mmol) was added. Subsequently, the mixture was stirred at room temperature for 2 h and then was heated to 40°C. Ethyl bromide (0.54 g, 5 mmol) was injected through a syringe in 15 min. The mixture was stirred at 80°C for 12 h and then water (15 mL) was added dropwise slowly. The organic phase was separated and the aqueous layer was extracted with dichloromethane. The combined organic layer was washed with water, dried over anhydrous sodium sulfate, filtered and the solvent was removed by rotary evaporation. The crude product was purified by column chromatography (silica gel, petroleum ether/ethyl acetate: 4/1) to give a white solid. Yield: 0.91 g, 63.8%. ^{1}H NMR (400 MHz, $CDCl_3$, δ): 7.97 (s, 0.5H), 7.64 (dd, J = 33.5, 8.3 Hz, 5H), 7.47-7.40 (m, 1H), 7.31 (d, J = 8.6 Hz, 0.5H); 4.26 (m, 2H); 1.47 (m, 3H).

5-Bromo-2-(4-bromophenyl)-1-(3-sulfonylpropyl)-1H-benzo[d]imidazole (monomer 2)

Under argon atmosphere, 5-bromo-2-(4-bromophenyl)-1H-benzo[d]imidazole(3) (0.7 g, 2 mmol) in DMF (10 mL) were stirred at 0°C and sodium hydride (60%) (0.32 g, 8 mmol) was added. Subsequently, the mixture was stirred at room temperature for 2 h and then was heated to 40°C. 1,3-Propanesultone (0.49 g, 4 mmol) dissolved in 5 mL DMF was added dropwise in 30 min. Subsequently, the reaction solution was stirred at 90°C for 12 h and cooled to room temperature. The mixture was poured into absolute ether (150 mL) and the precipitate was collected. The crude product was dried under vacuum at 60°C for 12 h and was purified by recrystallization from aqueous solution of potassium chloride to give a white solid. Finally this solid was dried under vacuum overnight again. Yield: 0.56 g, 56.4%. ^{1}H NMR (400 MHz, DMSO-d_6, δ): 8.04 (d, J = 1.7 Hz, 0.5H), 7.89 (d, J = 1.8 Hz, 0.5H); 7.82-7.62 (m, 5H); 7.42 (ddd, J = 22.8, 8.6, 1.8 Hz, 1H); 4.46 (dd, J = 15.0, 6.5 Hz, 2H); 2.39 (td, J = 7.1, 3.7 Hz, 2H); 2.0-1.93 (m, 2H).

2.2.2 Synthesis of polymers

(+)-PPBIPV

Under argon atmosphere, monomer 1 (0.29 g, 0.5 mmol), (+)-DVB (0.18 g, 0.5 mmol), palladium acetate (0.011 g, 0.05 mmol), tri(o-tolyl)phosphine (0.061 g, 0.2 mmol) and diisopropylamine (2 mL), toluene (1.5 mL) and DMSO (2 mL) was stirred in a two-neck flask at 100°C for 6 h. The reaction mixture was filtered and the filtrate was poured into the mixed solvent (ethyl ether/acetone/methanol: 8/6/1). The precipitate was filtered and then redissolved in DMSO (10 mL). The resulting solution was dialyzed against deionized water for 3 days using a 4kD MWCO cellulose membrane. Finally, the solvent was removed by rotary evaporation and the crude product was further dried under vacuum at 60°C for 48 h to give a yellow solid. Yield: 0.1128 g, 27.3%. ^{1}H NMR (400 MHz, DMSO-d_6, δ): 8.16-7.34 (m, 13H), 4.84-4.24 (m, 6H), 3.91 (s, 4H), 3.51 (s, 12H), 1.65-0.81 (m, 21H).

(-)-PPBIPV

Under argon atmosphere, the mixture solution of monomer 2 (0.25 g, 0.5 mmol), C4-DVB (0.14 g, 0.5 mmol), palladiumacetate (0.011 g, 0.05 mmol), tri(o-tolyl) phosphine (0.061 g, 0.2 mmol) and diisopropylamine (2.5 mL) and DMF (3 mL) was stirred at 100°C for 6 h. The reaction mixture was poured into methanol (20 mL) with dimethylglyoxime (0.158 g) and stirred for 10 min. The mixture solution was filtered and the filtrate was poured into the mixed solvent (ethyl ether/acetone: 1/1). The precipitate was filtered and then redissolved in DMSO (10 mL). The resulting solution was dialyzed against deionized water for 3 days using a 4kD MWCO cellulose membrane. Finally, the solvent was removed by rotary evaporation and the crude product was further dried under vacuum at 60°C for 48 h to give a yellow-brown solid. Yield: 0.1387 g, 43.4%. ^{1}H NMR (400 MHz, DMSO-d_6, δ): 8.13-6.87 (m, 13H), 4.55 (s, 2H), 4.12 (d, J = 37.1 Hz, 4H), 2.25-0.61 (m, 18H).

3 Results and discussion

3.1 Synthesis and characterization of monomers and polymers

The synthetic schemes for the monomers and the polymers are outlined in Scheme 1. During the formation of the imidazole ring, the position of the bromine substituent on the benzimidazole ring will be at the 4th or 5th position due to the different positions of oxidative dehydrogenation, and therefore compound 3 is a mixture. Of course, monomer 1 and monomer 2 derived from the nitrogen alkylation of compound 3 are also mixtures.

The polymerization of the two polymers were both carried out via Heck coupling reaction using $Pd(OAc)_2$ as catalyst and $P(o\text{-tolyl})_3$ as the corresponding ligand (31). Taking into account the presence of water soluble

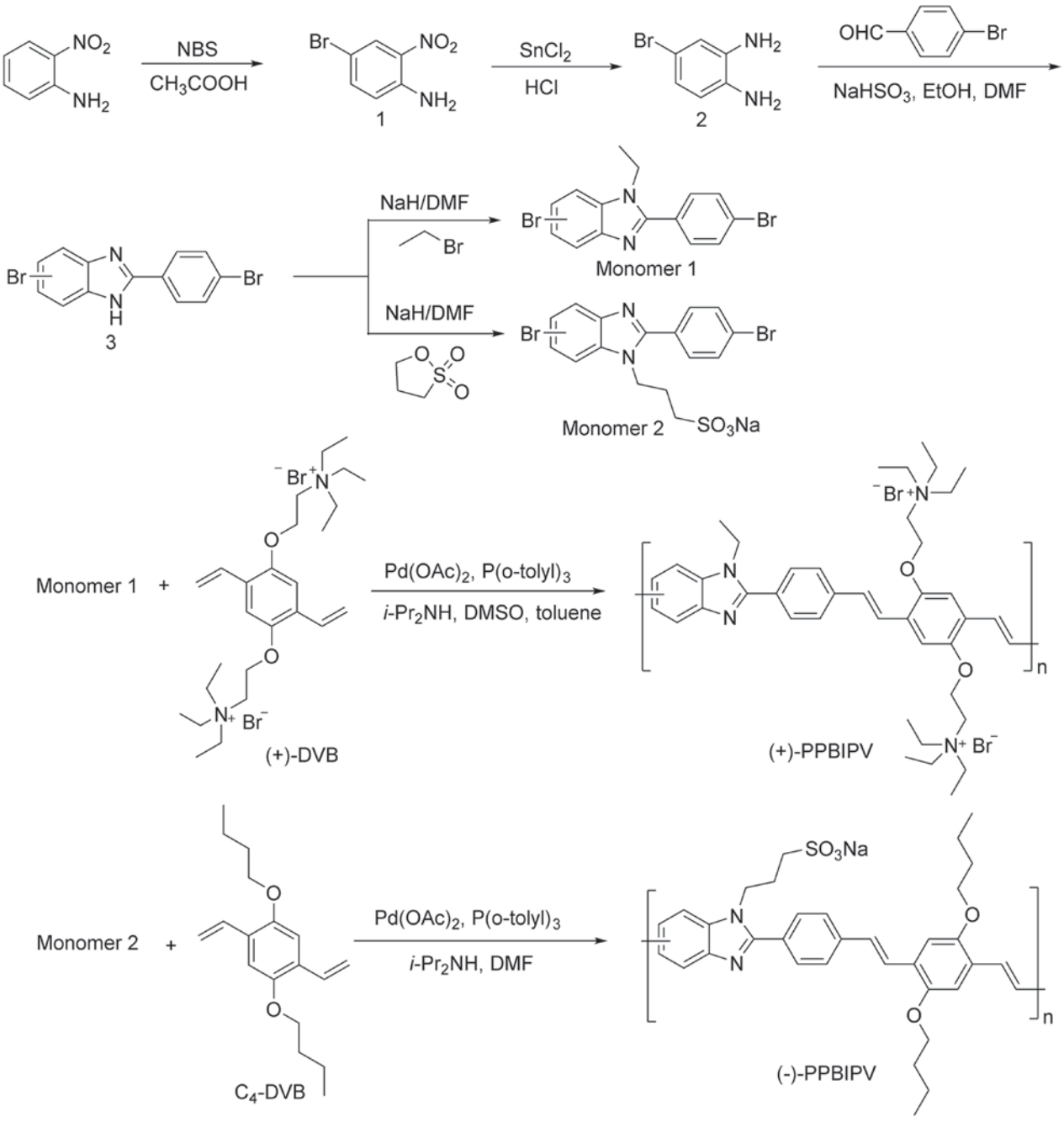

Scheme 1: Synthetic routes of monomers and polymers.

monomers and oil soluble monomers, we chose DMF that can dissolve most of the substances as solvent. During the procedure of the copolymerization, the conjugated length of (+)-PPBIPV and (-)-PPBIPV which was detected by the UV–vis spectrum was adjusted to be almost identical by controlling the polymerization time.

As shown in Figure 1, it can be seen that the characteristic peaks of polymer (+)-PPBIPV correspond well with the characteristic peaks of each monomer. Specifically, in the ^{1}H NMR spectrum of (+)-PPBIPV, the presence of the peaks at 0.81-1.65 ppm is attributed to the characteristic peak of the methyl group in the alkyl side chain of monomer 1 and (+)-DVB; the peaks at 3.51 ppm and 3.91 ppm are all attributed to the hydrogen of N-CH_2 on the quaternary ammonium group in (+)-DVB; the peaks at 4.24-4.84 ppm are respectively attributed to O-CH_2 of (+)-DVB unit and N-CH_2 of monomer 1 unit. Since the polymer is not a single pure material but a mixture of different molecular weights, a broad peak usually appears in the NMR spectrum of the polymer. Furthermore, the polymer is a compound with a large delocalized π bond, hydrogen atoms in the conjugated structure are often subjected to complex de-shielding effects, so the peaks at 7.34-8.16 ppm are the peaks of aromatic hydrogen atoms in the polymer backbone.

Figure 2 shows the ^{1}H NMR spectra of monomer 2, C4-DVB and (-)-PPBIPV. In the ^{1}H NMR spectrum of (-)-PPBIPV, the presence of the peaks at 0.56-2.10 ppm is attributed to the signal peaks generated by hydrogen atoms not adjacent to oxygen and nitrogen atoms on the alkyl side chains, showing the monomer 2 and C4-DVB units have been introduced into the main chain of (-)-PPBIPV. These results can also be found in the spectrum of (+)-PPBIPV in Figure 1. Moreover, the hydrogen atoms adjacent to oxygen and nitrogen atoms in the alkyl side chain appear at 3.84-4.55 ppm, and the signals in the region of 6.97-8.09 ppm are due to the hydrogen atoms of benzene ring.

It is well-known that CPEs can aggregate in its solution and that aggregated polymers can be easily absorbed on the chromatographic column, so precise molecular weight information of CPEs is difficult to obtain from

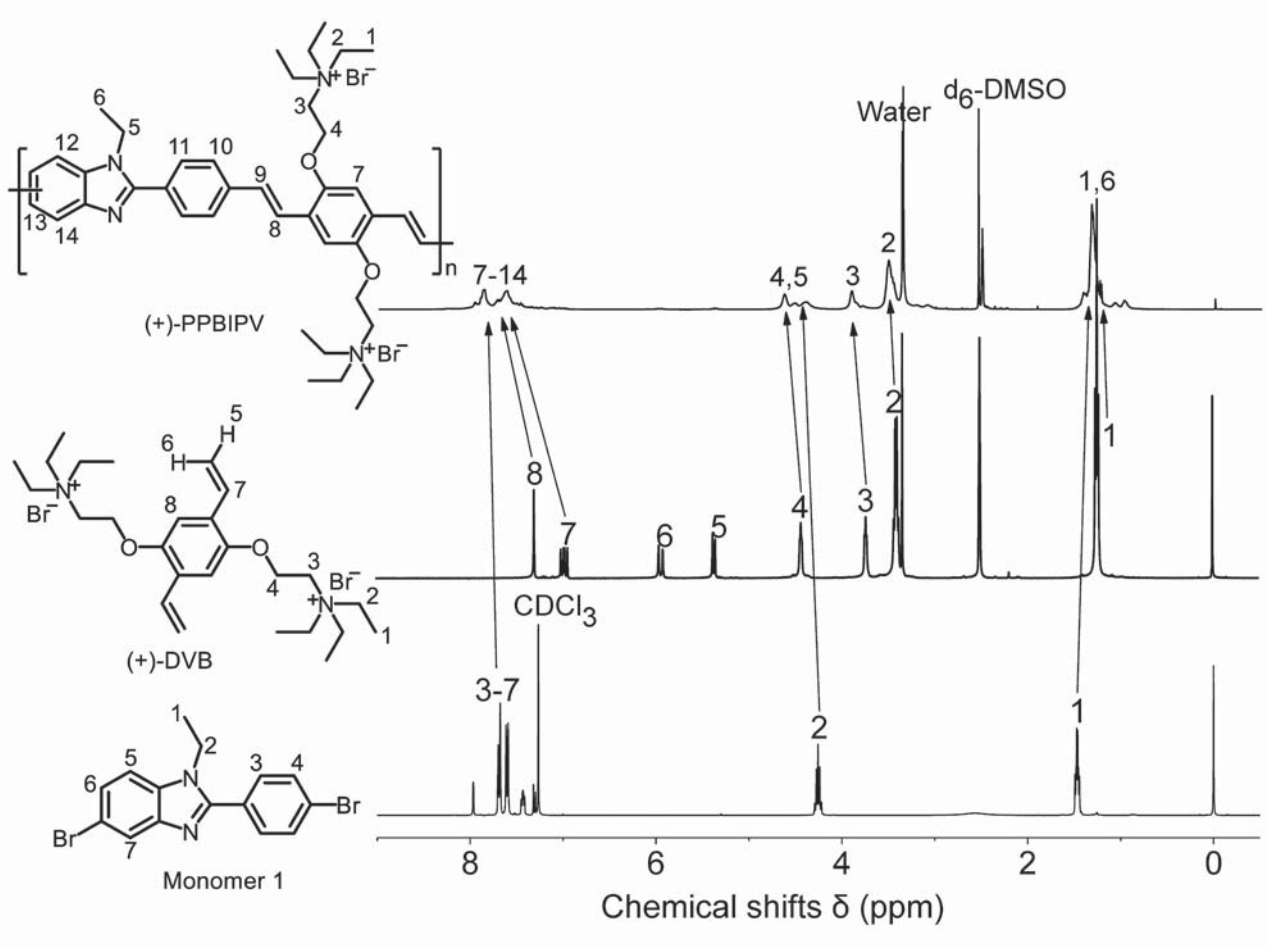

Figure 1: ^{1}H NMR spectra of monomer 1, (+)-DVB and (+)-PPBIPV.

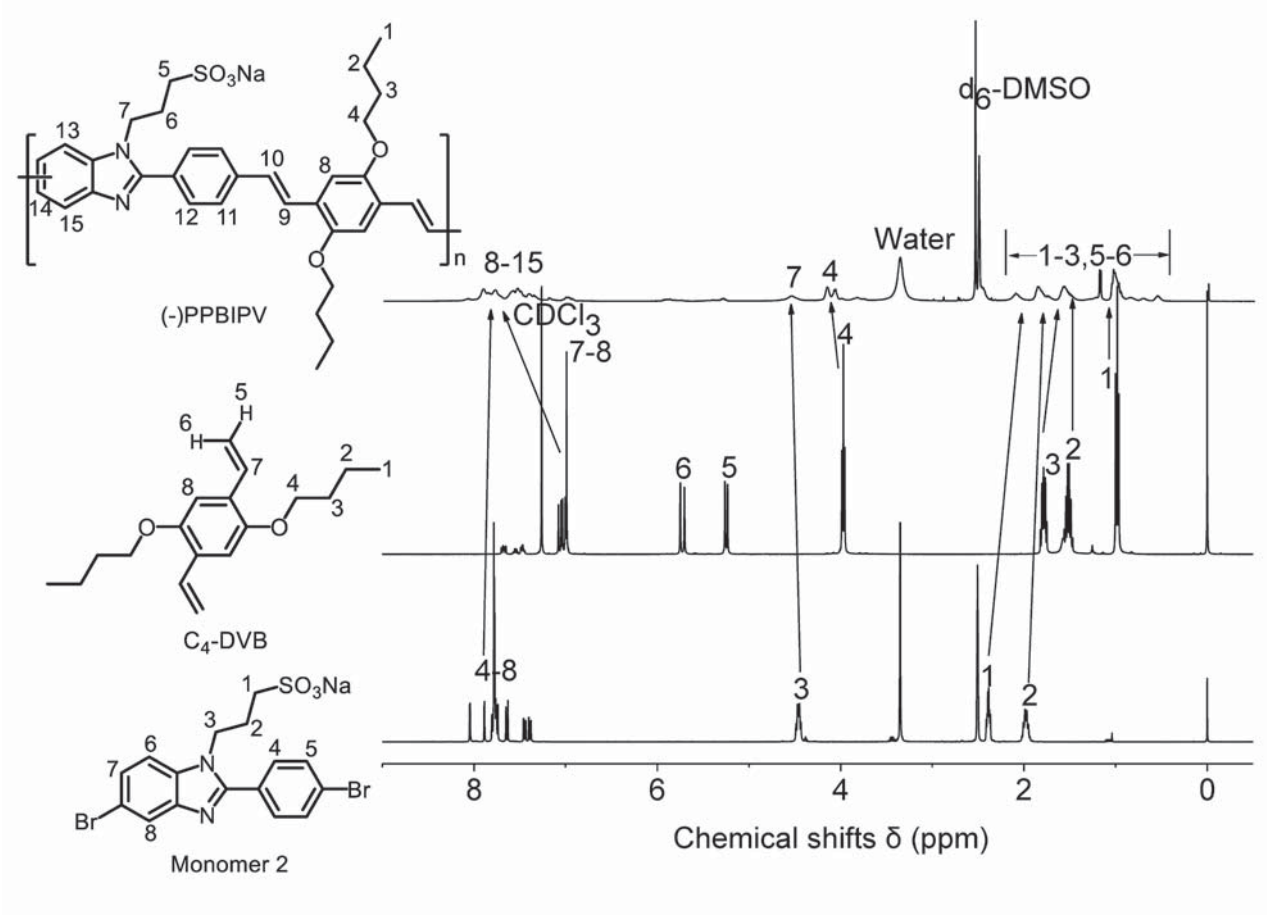

Figure 2: ^{1}H NMR spectra of monomer 2, C4-DVB and (-)-PPBIPV.

gel permeation chromatography (GPC). Another reason is that it is difficult to find a suitable solvent to conform to the measurement requests. Furthermore, owing to the aggregation phenomenon of CPEs, light scattering which is the common technique to measure the molecular weight as same as GPC is not available (32,33). Thus, the solutions of (+)-PPBIPV and (-)-PPBIPV were dialyzed by 4kD MWCO cellulose membrane, which ensured that the molecular weight of polymers were more than 4000 (at least eight repeating units). Although we can only get a general result in this way, but it is enough to prove that the polymerization of the two CPEs has been completed successfully and satisfied the requirement of photophysics and sensing measurement.

3.2 Basic photophysical properties of polymers

The absorption and emission data of monomer 1, monomer 2, (+)-DVB, C4-DVB, (+)-PPBIPV and (-)-PPBIPV are listed in Table 1. In the water, (+)-PPBIPV shows broad absorption band covered 300-500 nm visible light region and the absorption maximum at 415 nm. This phenomenon is associated with the increasing conjugate chain of the polymer, which decreases the energy from ground state to excited state. The fluorescence of (+)-PPBIPV is green in the solution, while the fluorescence of (+)-DVB and monomer 1 is purple, and its fluorescence intensity is significantly stronger than two monomers. In comparison with monomer 1, the PL emission maximum of (+)-PPBIPV at 501 nm showing red shifted 139 nm is attributed to its increasing conjugation degree. In addition, the maxima of absorption peak and fluorescence emission peak of (+)-PPBIPV are much larger than those of monomer 1 and (+)-DVB, which verifies the success of the polymerization.

As same as (+)-PPBIPV, the UV-vis and PL maxima of (-)-PPBIPV both show large red shifts compared to its monomers. (-)-PPBIPV exhibits the absorption maximum at 408 nm and emission maximum at 613 nm in the water. There is almost no overlap between the ultraviolet absorption band and the fluorescence emission band of (-)-PPBIPV, and the Stokes shift reaches 205 nm, which

can effectively prevent fluorescence self-absorption and exhibit the potential of fluorescence sensor materials.

The absorption and emission maxima of (+)-PPBIPV and (-)-PPBIPV are listed in Table 1, while the photos of conjugated polyelectrolytes in different solvents are shown in Figure 3. As shown in Figure 3a, the maximum absorption peak of (+)-PPBIPV is located in 403 nm in methanol. However, it exhibits a red shift in water and DMSO, which is located in 415 nm and 417 nm, respectively. Similarly, when the solvent is changed from methanol to DMSO or water, the emission maximum has been red shifted from 470 nm (in methanol) to 480 nm (in DMSO) or 501 nm (in water). In addition, the PL emission intensity of (+)-PPBIPV is significant in both methanol and DMSO, but weak in aqueous solution. In water, (+)-PPBIPV aggregates strongly by π-π stacking as same as other conjugated polyelectrolytes (34), which means that the conjugated layers of the polyelectrolytes are stacked mutually. This aggregation causes the conjugated polyelectrolytes to reach a higher degree of conjugation, making it easier for excitons to transfer between the backbones (35). Thus, the fluorescence quenching of (+)-PPBIPV in water may be attributed to energy dissipation caused by excitons transfer.

Figure 3b shows that the maximum absorption peaks are located in 417 nm in DMSO, 408 nm in water, and 405 nm in methanol, respectively. In addition, the emission peak of (-)-PPBIPV is located in 500 nm in methanol, corresponding to the intrinsic emission (36). However, it is worth noting that the fluorescence of (-)-PPBIPV in aqueous solution is very weak, and the emission maximum has been red shifted from 408 nm to 613 nm, which is consistent with the reported anionic conjugated polyelectrolyte (36). In general, the peak at long wavelength corresponds to aggregation emission in water. The shape of emission peak and the fluorescence solvent dependence are also the same as other sulfonate-substituted conjugated polyelectrolytes (36,37). Compared to (+)-PPBIPV, the emission maximum of (-)-PPBIPV exhibits a greater red shift in water. This phenomenon

Table 1: Optical properties of (+)-DVB, C4-DVB, monomer 1, monomer 2, (+)-PPBIPV and (-)-PPBIPV.

Monomers/Polymers	Solvent	UV-vis max (nm)	PL max (nm)	Stokes Shift (nm)/(cm^{-1})
(+)-DVB	Water	331	387	56/178571
C4-DVB	Dichloromethane	346	398	52/192308
Monomer 1	Dichloromethane	303	362	59/169492
Monomer 2	Water	296	368	72/138889
(+)-PPBIPV	Water	415	501	86/116279
	Methanol	403	470	67/149254
	DMSO	417	480	63/158730
(-)-PPBIPV	Water	408	613	205/48780
	Methanol	405	500	95/105263
	DMSO	417	495	78/128205

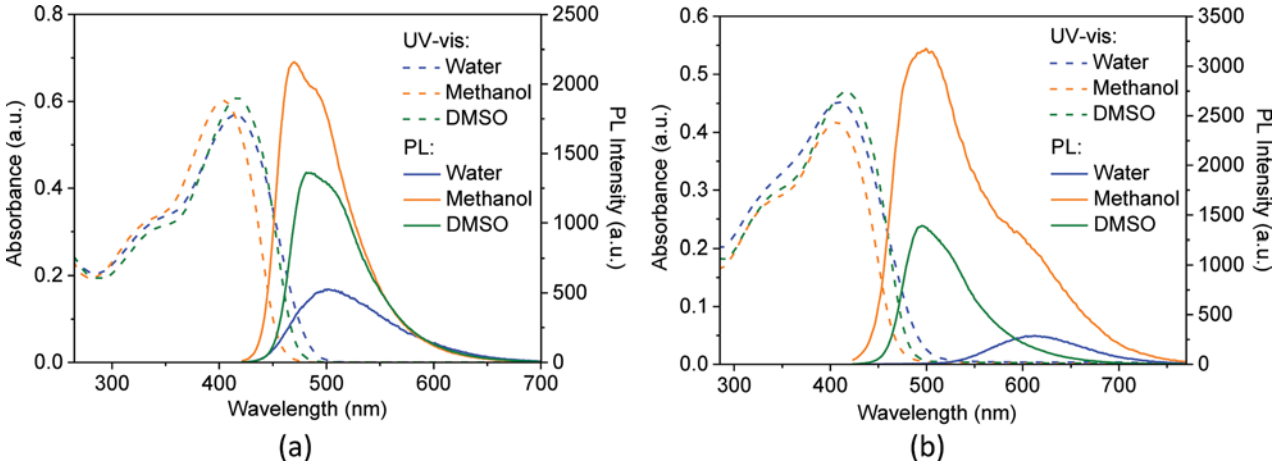

Figure 3: UV-vis and PL spectra of (+)-PPBIPV in water, methanol and DMSO (a); UV-vis and PL spectra of (-)-PPBIPV in water, methanol and DMSO (b).

can be attributed to the fact that (-)-PPBIPV has a stronger aggregation effect.

The fluorescence quantum yields (Φ) of (+)-PPBIPV and (-)-PPBIPV were measured by using quinine sulfate in 0.1 N sulfuric acid as standard (n = 1.336, Φ = 55%) according to the following equation (38):

$$\Phi_P = \left(\frac{n_P}{n_s}\right)^2 \cdot \frac{F_P}{F_S} \cdot \Phi_S \quad (1)$$

where the subscript P and S denote to polymer solution and standard, respectively. Φ is the fluorescence quantum yield, F is the intensity of fluorescence, and n is the refractive index of the solvent.

The Φ of (+)-PPBIPV and (-)-PPBIPV in methanol are 33% and 46%, respectively, which are basically consistent to the reference (39). However, the Φ of benzimidazole-based conjugated polymers is nearly 80% in THF (24). As reference reported, conjugate polyelectrolytes have lower fluorescence quantum yields than the uncharged oil soluble conjugated polymers of the same main-chain units (39). This phenomenon can be attributed to the fact that (+)-PPBIPV and (-)-PPBIPV aggregate strongly in the solvent, resulting in relatively low fluorescence quantum yields. On the other hand, the benzimidazole units of (+)-PPBIPV and (-)-PPBIPV are fluorescent chromophores, so their fluorescence quantum yields are higher than other PPV-type conjugated polyelectrolytes (40).

3.3 Metal ions response of polymers

The fluorescence responses of (+)-PPBIPV and (-)-PPBIPV on various metal ions were investigated. The solutions of metal ion were prepared by $PdCl_2$, $FeCl_3 \cdot 6H_2O$, $MgCl_2 \cdot 6H_2O$, $SnCl_2 \cdot 2H_2O$, $CoCl_2 \cdot 6H_2O$, $ZnCl_2$, $CuSO_4 \cdot 5H_2O$, $MnSO_4 \cdot H_2O$, $NiCl_2 \cdot 6H_2O$, $Cr(NO_3)_3 \cdot 9H_2O$, $FeSO_4 \cdot 7H_2O$, $HgCl_2$ and $CdCl_2$, respectively. All of the concentrations of polymers were 2×10^{-5} mol/L. In metal ion fluorescence sensing experiments (Figure 4 and Figure 7), when the metal ion is added to the polymer solution and the fluorescence intensity of the solution no longer changes, the ion concentration is called the limiting concentration.

3.4 Sensing properties of (+)-PPBIPV

Figure 4a shows the PL spectra of aqueous solution of (+)-PPBIPV with Fe^{2+}, Zn^{2+}, Cd^{2+}, Cr^{3+}, Hg^{2+}, Co^{2+}, Mg^{2+}, Mn^{2+}, Ni^{2+}, Cu^{2+}, Sn^{2+} and Fe^{3+}. The PL max (nm) and maxima of fluorescence intensity of (+)-PPBIPV with different metal ions are listed in Table 2. It can be found that Fe^{3+}, Sn^{2+}, Cr^{3+} and Hg^{2+} can reduce the fluorescence of (+)-PPBIPV, but the decrease occurs most notably upon the addition of Fe^{3+}. On the contrary, there is a small increase in fluorescence intensity of (+)-PPBIPV in the presence of Fe^{2+} and Cu^{2+}. And other metal ions hardly lead to changes in PL spectrum of (+)-PPBIPV. The fluorescence-quenching ratios (I_0/I_1-1) of aqueous solution of (+)-PPBIPV in the presence of different metal ions are shown in Figure 4c. It should be mentioned that even if the fluorescence quenching ratios of Sn^{2+} and Cr^{3+} are 0.34 and 0.25, respectively, they are still small compared to 1.52 of Fe^{3+}. These results show that (+)-PPBIPV has better fluorescent sensitivity to Fe^{3+} in aqueous solution.

The PL spectra of methanol solution of (+)-PPBIPV with various metal ions (Fe^{2+}, Zn^{2+}, Cd^{2+}, Cr^{3+}, Hg^{2+}, Co^{2+}, Mg^{2+}, Mn^{2+}, Ni^{2+}, Cu^{2+}, Sn^{2+}, Fe^{3+} and Pd^{2+}) were also investigated (Figure 4b). Pd^{2+} exhibits the greatest effect on the fluorescence of (+)-PPBIPV methanol solution, which almost completely quenches the fluorescence of the polymer with a quenching rate as high as 99%. Moreover, Cu^{2+}, Sn^{2+}, Fe^{2+} and Fe^{3+} can partially quench the solution fluorescence and their quenching rates are 72%, 55%, 44% and 34%, respectively. As shown in Figure 4d, the fluorescence quenching ratio of Pd^{2+} is much larger than other metal ions, indicating that (+)-PPBIPV has high selectivity and excellent sensitivity for Pd^{2+} in the methanol solution.

Figure 5a gives the fluorescence spectra of (+)-PPBIPV in water with different concentrations of Fe^{3+}. As the concentration of Fe^{3+} increases, the fluorescence intensity of (+)-PPBIPV is quenched from 2611 to 1121. The fluorescence quenching efficiency of (+)-PPBIPV can be described by the Stern-Volmer equation (41): $I_0/I_1 = 1 + K_{SV}[Q]$, where I_0 and I_1 are the fluorescence intensities of the system in the absence and presence of Fe^{3+}, respectively, K_{SV} is the Stern-Volmer quenching constant, and [Q] is the Fe^{3+} concentration. At the concentrations of Fe^{3+} between 0 and 162 μM, a Stern-Volmer plot of the fluorescence intensity of (+)-PPBIPV versus the concentration of Fe^{3+} is linear with a K_{SV} value of 7.78×10^3 M^{-1}, as shown in Figure 5b. The I_0/I_1 versus [Fe^{3+}] is a straight line, indicating that there is only a single quenching mechanism in this system. Investigating the fluorescence sensor based on benzimidazole, it is found that the quenching mechanism is generally forming a complex between the sp^2 nitrogen atom and the metal ions (42). Therefore, the mechanism of fluorescence

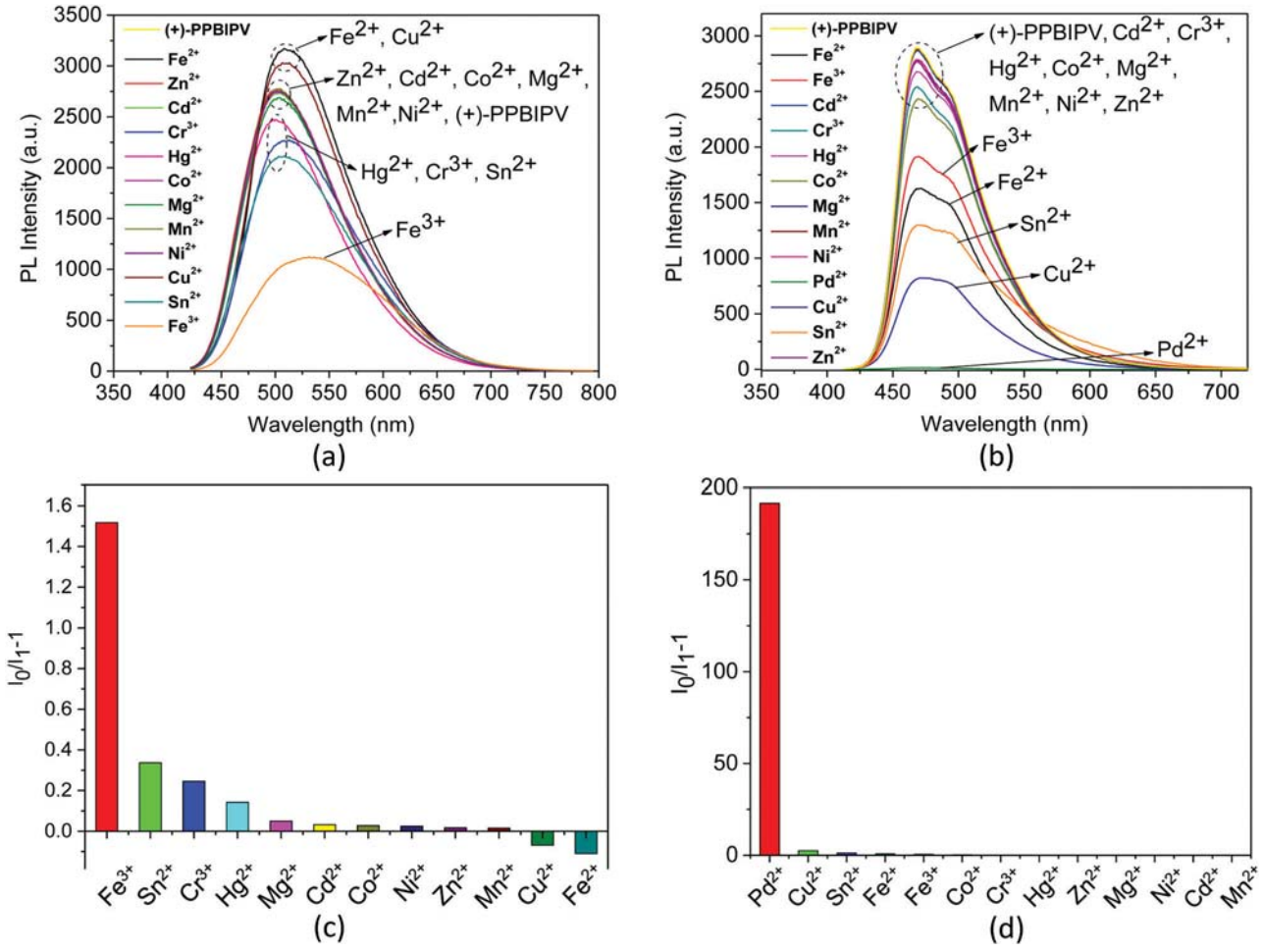

Figure 4: PL spectra of aqueous solution of (+)-PPBIPV with different metal ions (a); PL spectra of methanol solution of (+)-PPBIPV with different metal ions (b); PL quenching ratios (I_0/I_1-1) of aqueous solution of (+)-PPBIPV with different metal ions (c); PL quenching ratios (I_0/I_1-1) of methanol solution of (+)-PPBIPV with different metal ions (d).

Table 2: PL max (nm) and maxima of fluorescence intensity of (+)-PPBIPV with different metal ions.

(+)-PPBIPV in water			(+)-PPBIPV in methanol		
Metal ion	**PL max (nm)**	**Fluorescence intensity (a.u.)**	**Metal ion**	**PL max (nm)**	**Fluorescence intensity (a.u.)**
blank	500	2822	blank	470	2889
Cu^{2+}	507	3030	Cu^{2+}	471	821
Fe^{3+}	532	1121	Fe^{3+}	470	1915
Hg^{2+}	500	2471	Hg^{2+}	468	2678
Cd^{2+}	504	2734	Cd^{2+}	469	2870
Zn^{2+}	502	2774	Zn^{2+}	469	2772
Co^{2+}	506	2746	Co^{2+}	469	2434
Ni^{2+}	501	2753	Ni^{2+}	469	2785
Mg^{2+}	503	2688	Mg^{2+}	468	2784
Cr^{3+}	508	2265	Cr^{3+}	469	2542
Mn^{2+}	504	2779	Mn^{2+}	470	2881
Fe^{2+}	508	3171	Fe^{2+}	472	1627
Sn^{2+}	503	2111	Sn^{2+}	471	1297
			Pd^{2+}	473	15

quenching of (+)-PPBIPV towards Fe^{3+} is static quenching in water. The stoichiometric relationship between Fe^{3+} and (+)-PPBIPV can be determined by the Benesi-Hildebrand expression based on fluorescence spectra (43): $1/(F_0\text{-}F) = 1/(K(F_0\text{-}F_{min})[Q]^n) + 1/(F_0\text{-}F_{min})$, where F_0 and F are the fluorescence intensities in the absence and presence of Fe^{3+}, respectively, F_{min} is the minimum fluorescence intensity in the presence of Fe^{3+}, and K is the association constant. The measured fluorescence intensity $[1/(F_0\text{-}F)]$ varies as a function of $1/[Fe^{3+}]$ (n = 1) in a linear (R^2 = 0.98894), indicating 1:1 stoichiometry between (+)-PPBIPV and Fe^{3+} (Figure 5c). Furthermore, the K obtained from the slope and intercept of the line is 1.47×10^4 M^{-1} for (+)-PPBIPV binding to Fe^{3+}.

Subsequently, we investigated the ability of methanol solution (+)-PPBIPV to detect Pd^{2+}. As Figure 6a shows, the fluorescence intensity of (+)-PPBIPV decreases regularly as the concentration of Pd^{2+} increases, from 0 to 60 μM. As shown in Figure 6b, a Stern-Volmer plot of the fluorescence intensity of (+)-PPBIPV versus the concentration of Pd^{2+} is a upward curve instead of a straight line, which indicates the fluorophore is quenched by both dynamic quenching and static quenching with Pd^{2+}. On the other hand, when the concentration of Pd^{2+} is between 0 and 15 μM, a Stern-Volmer plot of the fluorescence intensity of (+)-PPBIPV versus the concentration of Pd^{2+} is linear with a K_{SV} value of 5.93×10^4 M^{-1}, indicating the mechanism of fluorescence quenching of methanol solution (+)-PPBIPV towards Pd^{2+} is static quenching in the low concentration region. Meanwhile, Benesi-Hildebrand plots of the fluorescence titration combined with (+)-PPBIPV and Pd^{2+} is yielded linear correlation coefficients of 0.99581, using the Benesi-Hildebrand equation of linear fitting based on 1:1 binding (n = 1) (Figure 6c). The strong correlation proves that there is 1:1 binding between (+)-PPBIPV and Pd^{2+}, and the K is calculated as 1.02×10^4 M^{-1}.

All of the measurement methods of (-)-PPBIPV are the same as (+)-PPBIPV. The PL max (nm) and maxima of

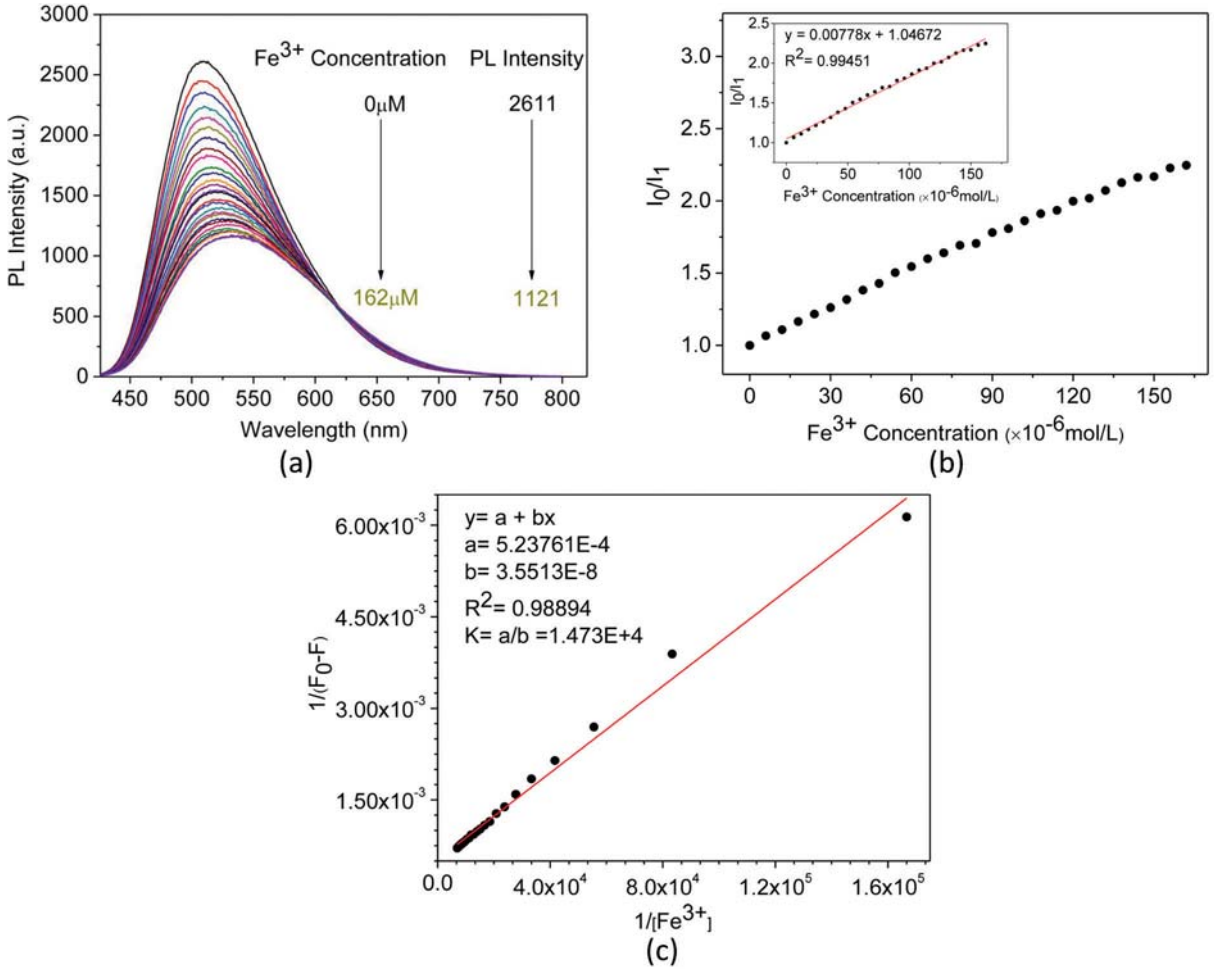

Figure 5: PL spectra of aqueous solution of (+)-PPBIPV with different concentrations of Fe^{3+} (a); PL titration curves of aqueous solution of (+)-PPBIPV with Fe^{3+} (b); The Benesi-Hildebrand plot of aqueous solution of (+)-PPBIPV with Fe^{3+} (c).

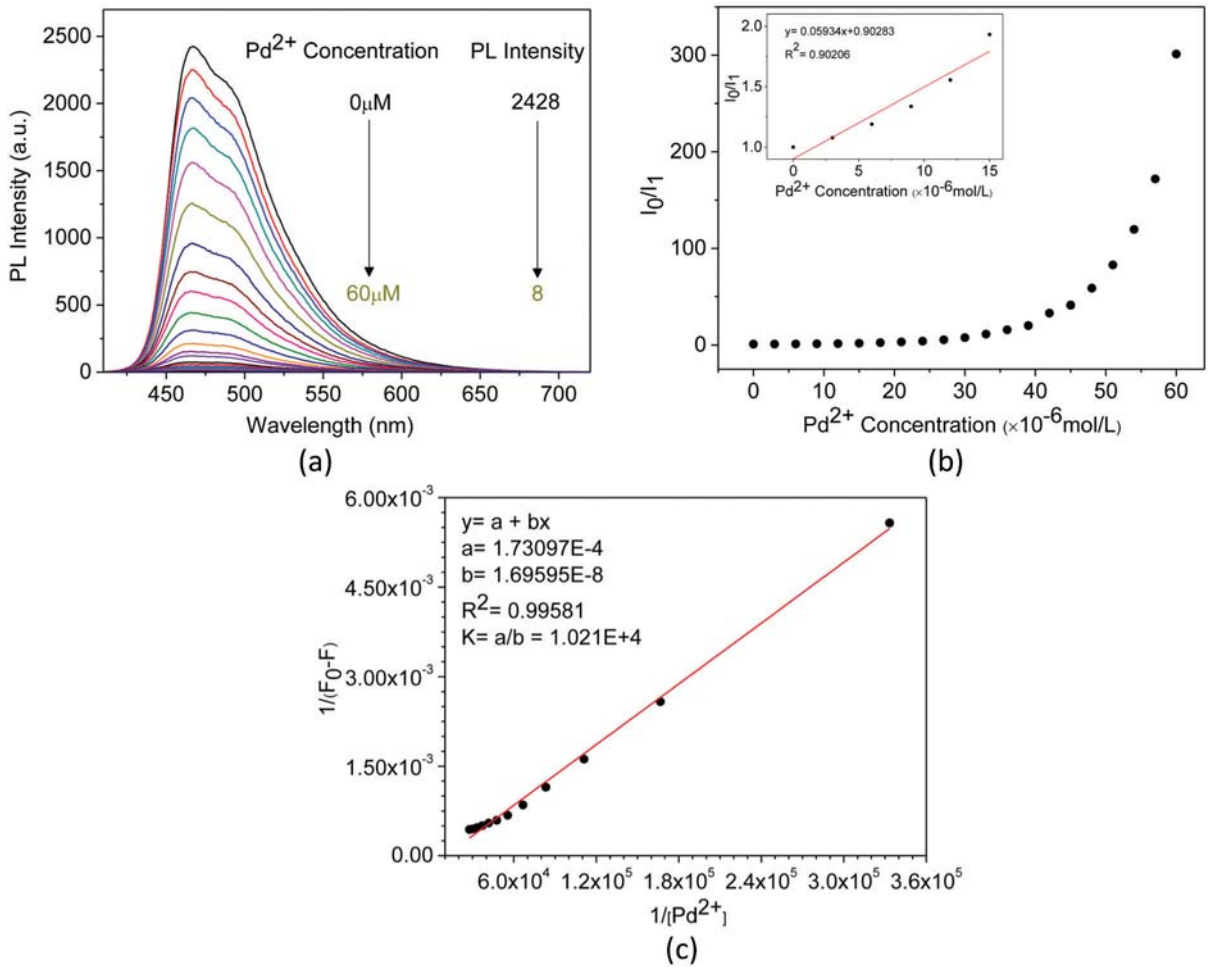

Figure 6: PL spectra of methanol solution of (+)-PPBIPV with different concentrations of Pd^{2+} (a); PL titration curves of methanol solution of (+)-PPBIPV with Pd^{2+} (b); The Benesi-Hildebrand plot of methanol solution of (+)-PPBIPV with Pd^{2+} (c).

Table 3: PL max (nm) and maxima of fluorescence intensity of (-)-PPBIPV with different metal ions.

(-)-PPBIPV in water			(-)-PPBIPV in methanol		
Metal ion	**PL max (nm)**	**Fluorescence intensity (a.u.)**	**Metal ion**	**PL max (nm)**	**Fluorescence intensity (a.u.)**
blank	613	3126	blank	500	8576
Cu^{2+}	612	1575	Cu^{2+}	505	1529
Fe^{3+}	613	2894	Fe^{3+}	531	210
Hg^{2+}	610	2898	Hg^{2+}	508	1961
Cd^{2+}	611	2911	Cd^{2+}	500	7167
Zn^{2+}	609	2950	Zn^{2+}	504	2726
Co^{2+}	615	3050	Co^{2+}	502	4707
Ni^{2+}	613	3068	Ni^{2+}	501	6198
Mg^{2+}	613	3139	Mg^{2+}	502	7101
Cr^{3+}	614	3213	Cr^{3+}	603	358
Mn^{2+}	610	3277	Mn^{2+}	502	6635
Fe^{2+}	611	3911	Fe^{2+}	509	2819
Sn^{2+}	613	5430	Sn^{2+}	614	564
			Pd^{2+}	510	369

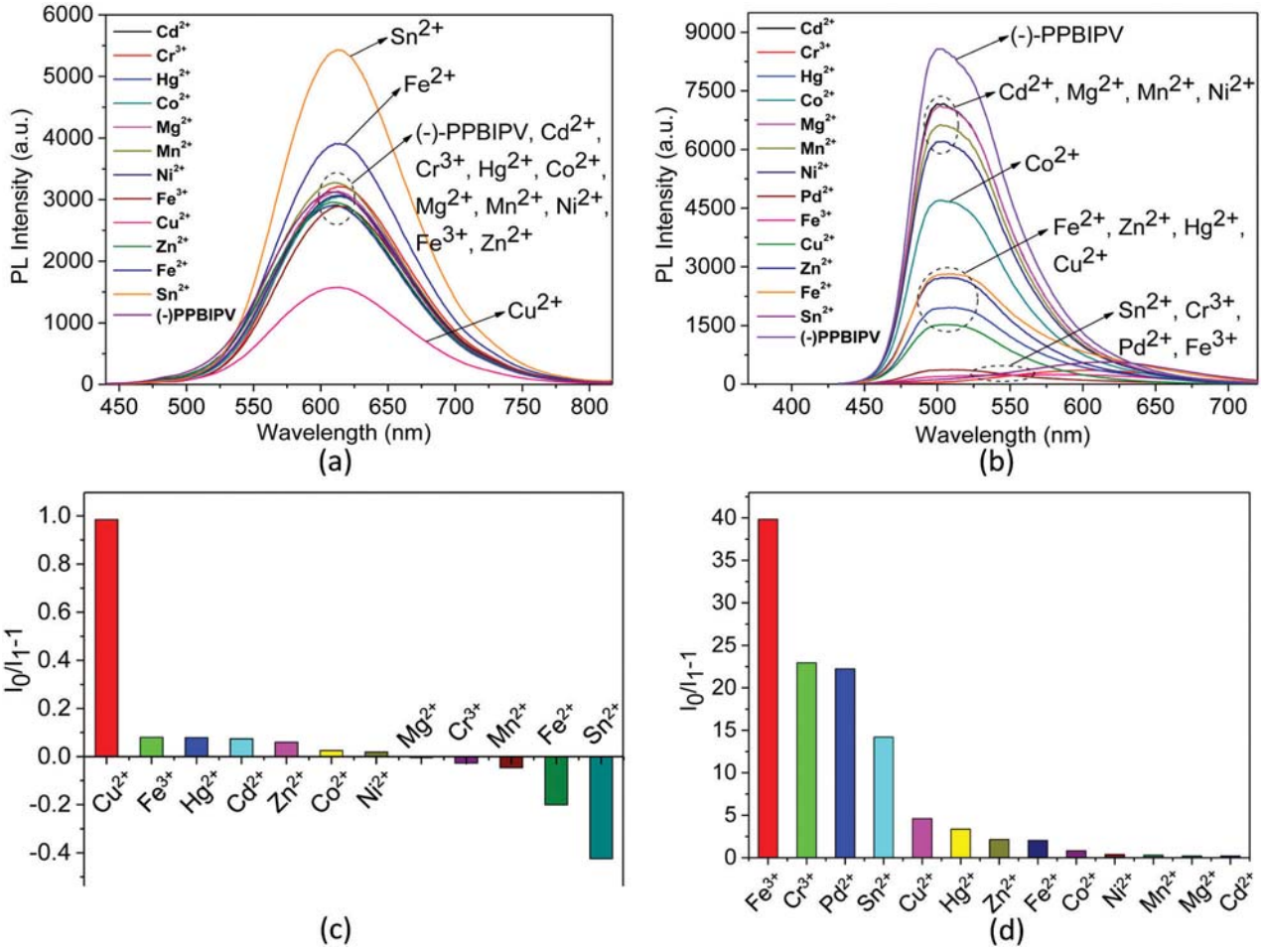

Figure 7: PL spectra of aqueous solution of (-)-PPBIPV with different metal ions (a); PL spectra of methanol solution of (-)-PPBIPV with different metal ions (b); PL quenching ratios (I_0/I_1-1) of aqueous solution of (-)-PPBIPV with different metal ions (c); PL quenching ratios (I_0/I_1-1) of methanol solution of (-)-PPBIPV with different metal ions (d).

fluorescence intensity of (-)-PPBIPV with different metal ions are listed in Table 3. As shown in Figures 7a and 7c, Cu^{2+} can quench the fluorescence of aqueous solution of (-)-PPBIPV by nearly 50%. Zn^{2+}, Cd^{2+}, Cr^{3+}, Hg^{2+}, Co^{2+}, Mg^{2+}, Mn^{2+}, Ni^{2+} and Fe^{3+} exhibit little or no effect on the fluorescence intensity of the polymer. Both Fe^{2+} and Sn^{2+} can increase the fluorescence, but Sn^{2+} is more obviously, which doubles the fluorescence intensity of the polymer approximately.

Figure 7b shows the PL spectra of methanol solution of (-)-PPBIPV with different metal ions. Metal ions response of methanol solution of (-)-PPBIPV is more complicated than aqueous solution of (-)-PPBIPV. According to Figure 7d, the methanol solution of (-)-PPBIPV has certain selectivity for Fe^{3+}, Pd^{2+}, Cr^{3+} and Sn^{2+}, especially Fe^{3+}.

As Figure 8a shows, adding 60 μM Sn^{2+} results in 100% fluorescence enhancement of (-)-PPBIPV. Moreover, the Stern-Volmer plot of the fluorescence intensity of (-)-PPBIPV versus the concentration of Sn^{2+} is a downward curve, which can also be fitted as the equation approximatively, y = -0.01325x + 0.93436 (Figure 8b). In this system, the addition of Sn^{2+} increases the fluorescence intensity of (-)-PPBIPV, so the Benesi-Hildebrand equation takes this form (44): $1/(F\text{-}F_0) = 1/(K(F_{max}\text{-}F_0)[Q]^n) + 1/(F_{max}\text{-}F_0)$, where F_0 and F are the fluorescence intensities in the absence and presence of Sn^{2+}, respectively, F_{max} is the maximum fluorescence intensity in the presence of Sn^{2+}, and K is the association constant. The Benesi-Hildebrand equation fitting curves of the $1/(F\text{-}F_0)$ to $1/[Sn^{2+}]$ are shown in Figure 8c, yielded linear correlation coefficients of 0.99655. The result indicates 1:1 stoichiometry between (-)-PPBIPV and Sn^{2+}, with a K value of 1.81×10^4 M^{-1}.

Figure 9a shows the fluorescence spectra of the (-)-PPBIPV in methanol solution with the increasing

concentration of Fe^{3+}. Add 30 μM Fe^{3+}, causing the fluorescence of (-)-PPBIPV to be quenched 97.5%. As shown in Figure 9b, a Stern-Volmer plot of the fluorescence intensity of (-)-PPBIPV versus the concentration of Fe^{3+} is a non-liner, which is similar to the Stern-Volmer plot of the methanol solution of (+)-PPBIPV with Pd^{2+}. In the low concentration region, the mechanism of fluorescence quenching of methanol solution (-)-PPBIPV towards Fe^{3+} is static quenching with a K_{SV} value of 3.44×10^5 M^{-1}. From Figure 9c, the stoichiometric ratio of (-)-PPBIPV to Fe^{3+} in methanol solution is 1:1, and the association constant K is 5.39×10^4 M^{-1}, which is much larger than the association constant of (+)-PPBIPV and Fe^{3+} in aqueous solution ($K=1.47\times10^4$ M^{-1}). Except for the difference in solvent, the reason may be that the side chain of (-)-PPBIPV is a negatively charged sulfonic acid group, which has an electrostatic attraction with metal ions. This force causes a large amount of metal ions to aggregate around the polymer, so metal ions and polymer receptor units can be better combined.

4 Conclusions

In summary, two novel benzimidazole-based conjugated polyelectrolytes (+)-PPBIPV and (-)-PPBIPV have been designed, synthesized and characterized successfully. In metal sensing aspects, it is demonstrated that Fe^{3+} can remarkably reduce the fluorescence of (+)-PPBIPV in aqueous solution. When the concentration of Fe^{3+} is in the range of 6-66 μM, Fe^{3+} can be detected by (+)-PPBIPV quantitatively. Furthermore, Pd^{2+} can quench almost all the fluorescence intensity of the polymer in methanol solution, of which K_{SV} is 5.93×10^4 M^{-1}, and the results show that there are both static quenching and dynamic quenching in this system. In the low concentration region, there is a single

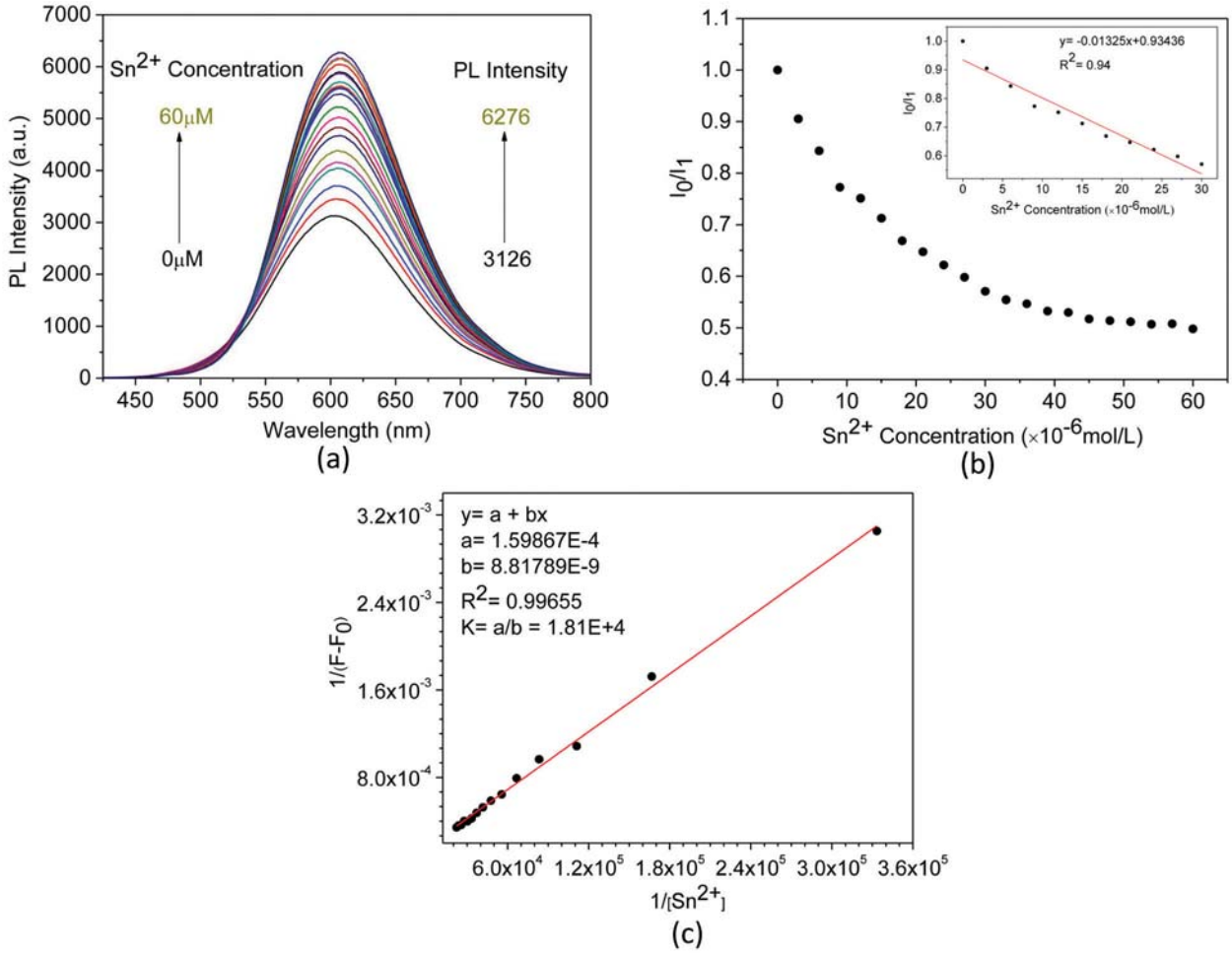

Figure 8: PL spectra of aqueous solution of (-)-PPBIPV with different concentration of Sn^{2+} (a); PL titration curves of aqueous solution of (-)-PPBIPV with Sn^{2+} (b); The Benesi-Hildebrand plot of aqueous solution of (-)-PPBIPV with Sn^{2+} (c).

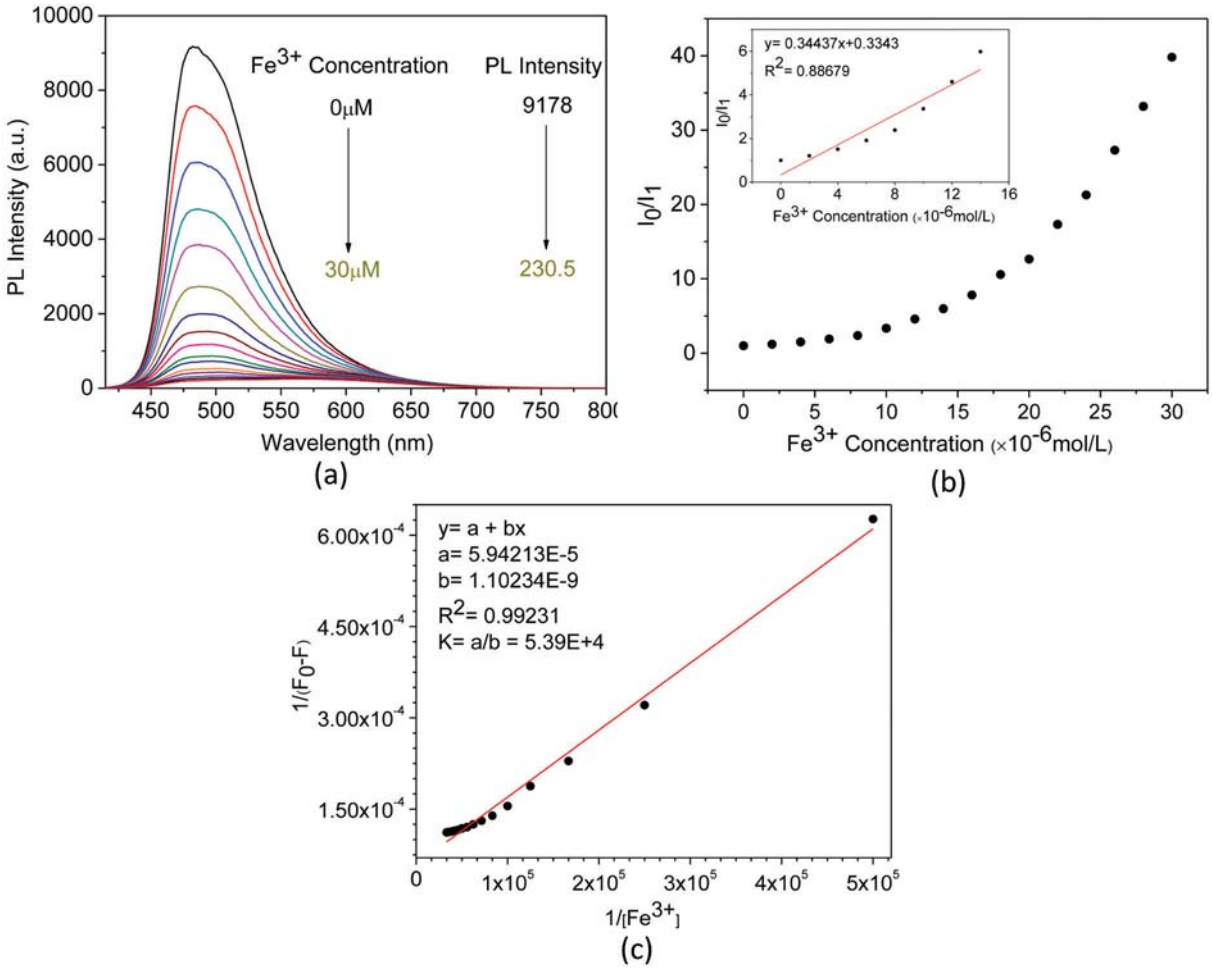

Figure 9: PL spectra of methanol solution of (-)-PPBIPV with different concentration of Fe^{3+} (a); PL titration curves of methanol solution of (-)-PPBIPV with Fe^{3+} (b); The Benesi-Hildebrand plot of methanol solution of (-)-PPBIPV with Fe^{3+} (c).

static quenching, and the stoichiometric ratio of (+)-PPBIPV and Pd^{2+} in methanol solution is 1:1. On the other hand, as for (-)-PPBIPV, Sn^{2+} can double the fluorescence of its aqueous solution, and the results shows that the stoichiometric relationship between (-)-PPBIPV and Sn^{2+} also is 1:1. Almost each ion can affect the fluorescence of (-)-PPBIPV in methanol solution, especially Fe^{3+}, of which the fluorescence quenching efficiency is 97.5%. The reason for this phenomenon may be attributed to the complexation of metal ions with (-)-PPBIPV and the electrostatic attraction between positive metal ions and negative charges in side-chain of the polymer. By analyzing and comparing their response to metal ions, the influence of side chain electrification on the sensing properties of conjugated polymers can be further discussed. All results show that these two conjugated polyelectrolytes could potentially be used as effective fluorescent sensors for detecting metal ions in biological and environmental media.

Acknowledgements: This work is financially supported by the "Shuangzhi" Project of Sichuan Agricultural University (No. 00770105) and the National University Student Innovation Program (No. 201910626096).

References

1. Duan C., Wang L., Zhang K., Guan X., Huang F., Conjugated zwitterionic polyelectrolytes and their neutral precursor as electron injection layer for high-performance polymer light-emitting diodes. Adv. Mater., 2011, 23, 1665-1669.
2. Seo J.H., Gutacker A., Sun Y., Wu H., Huang F., Cao Y., et al., Improved high-efficiency organic solar cells via incorporation of a conjugated polyelectrolyte interlayer. J. Am. Chem. Soc., 2011, 133, 8416-8419.
3. Liang J., Li K., Liu B., Visual sensing with conjugated polyelectrolytes. Chem. Sci., 2013, 4, 1377.
4. You J., Park T., Kim J., Heo J.S., Kim H.S., Kim H.O., et al., Highly fluorescent conjugated polyelectrolyte for protein sensing and cell-compatible chemosensing applications. ACS Appl. Mater. Inter., 2014, 6, 3305-3311.

5. Wang Y., Liu B., Mikhailovsky A., Bazan G.C., Conjugated polyelectrolyte-metal nanoparticle platforms for optically amplified DNA detection. Adv. Mater., 2010, 22, 656-659.
6. Sun P., Lu X., Fan Q., Zhang Z., Song W., Li B., et al., Water-Soluble Iridium(III)-Containing Conjugated Polyelectrolytes with Weakened Energy Transfer Properties for Multicolor Protein Sensing Applications. Macromolecules, 2011, 44, 8763-8770.
7. Xia F., Zuo X., Yang R., Xiao Y., Kang D., Vallee-Belisle A., et al., Colorimetric detection of DNA, small molecules, proteins, and ions using unmodified gold nanoparticles and conjugated polyelectrolytes. Proc. Natl. Acad. Sci. USA, 2010, 107, 10837-10841.
8. Kim B., Jung I.H., Kang M., Shim H.K., Woo H.Y., Cationic conjugated polyelectrolytes-triggered conformational change of molecular beacon aptamer for highly sensitive and selective potassium ion detection. J. Am. Chem. Soc., 2012, 134, 3133-3138.
9. Roy S., Gunukula A., Ghosh B., Chakraborty C., A folic acid-sensitive polyfluorene based "turn-off" fluorescence nanoprobe for folate receptor overexpressed cancer cell imaging. Sensor. Actuat. B-Chem., 2019, 291, 337-344.
10. Vazquez-Guillo R., Martinez-Tome M.J., Kahveci Z., Torres I., Falco A., Mallavia R., et al., Synthesis and Characterization of a Novel Green Cationic Polyfluorene and Its Potential Use as a Fluorescent Membrane Probe. Polymers, 2018, 10, 938-957.
11. Hussain S., Malik A.H., Iyer P.K., Highly precise detection, discrimination, and removal of anionic surfactants over the full pH range via cationic conjugated polymer: an efficient strategy to facilitate illicit-drug analysis. ACS Appl. Mater. Inter., 2015, 7, 3189-3198.
12. Park S., Jeong J. E., Le V. S., Seo J., Yu B., Kim D.Y., et al., Enhanced Electron Transfer Mediated by Conjugated Polyelectrolyte and Its Application to Washing-Free DNA Detection. J. Am. Chem. Soc., 2018, 140, 2409-2412.
13. Bojanowski N.M., Bender M., Seehafer K., Bunz U.H.F., Discrimination of Saccharides by a Simple Array. Chemistry, 2017, 23, 12253-12258.
14. Park Y., Liu Z., Routh P.K., Kuo C.Y., Park Y.S., Tsai H., et al., DNA-assisted photoinduced charge transfer between a cationic poly(phenylene vinylene) and a cationic fullerene. Phys. Chem. Chem. Phys., 2015, 17, 15675-15678.
15. Jurin F.E., Buron C.C., Clément S., Mehdi A., Viau L., Lakard B., et al., Flexible and conductive multilayer films based on the assembly of PEDOT:PSS and water soluble polythiophenes. Org. Electron. , 2017, 46, 263-269.
16. Huber R.C., Ferreira A.S., Thompson R., Kilbride D., Knutson N.S., Devi L.S., et al., Long-lived photoinduced polaron formation in conjugated polyelectrolyte-fullerene assemblies. Science, 2015, 348, 1340-1343.
17. Molina P., Tarraga A., Oton F., Imidazole derivatives: a comprehensive survey of their recognition properties. Org. Biomol. Chem., 2012, 10, 1711-1724.
18. Ajani O.O., Aderohunmu D.V., Ikpo C.O., Adedapo A.E., Olanrewaju I.O., Functionalized Benzimidazole Scaffolds: Privileged Heterocycle for Drug Design in Therapeutic Medicine. Arch. Pharm. Chem. Life Sci., 2016, 349, 475-506.
19. Ermler S., Scholze M., Kortenkamp A., Seven benzimidazole pesticides combined at sub-threshold levels induce micronuclei in vitro. Mutagenesis, 2013, 28, 417-426.
20. Saluja P., Sharma H., Kaur N., Singh N., Jang D.O., Benzimidazole-based imine-linked chemosensor: chromogenic sensor for Mg^{2+} and fluorescent sensor for Cr^{3+}. Tetrahedron, 2012, 68, 2289-2293.
21. Liu H., Zhang B., Tan C., Liu F., Cao J., Tan Y., et al., Simultaneous bioimaging recognition of Al^{3+} and Cu^{2+} in living-cell, and further detection of F^- and S^{2-} by a simple fluorogenic benzimidazole-based chemosensor. Talanta, 2016, 161, 309-319.
22. Kim Y.S., Lee J.J., Lee S.Y., Jo T.G., Kim C., A highly sensitive benzimidazole-based chemosensor for the colorimetric detection of Fe(ii) and Fe(iii) and the fluorometric detection of Zn(ii) in aqueous media. RSC Adv., 2016, 6, 61505-61515.
23. Velmurugan K., Mathankumar S., Santoshkumar S., Amudha S., Nandhakumar R., Specific fluorescent sensing of aluminium using naphthalene benzimidazole derivative in aqueous media. Spectrochim. Acta A, 2015, 139, 119-123.
24. Zhu H., Tong H., Gong Y., Shao S., Deng C., Yuan W.Z., et al., Fluorene- and benzimidazole-based blue light-emitting copolymers: Synthesis, photophysical properties, and PLED applications. J. Polym. Sci. A1, 2012, 50, 2172-2181.
25. Shim J.Y., Lee B.H., Song S., Kim H., Kim J.A., Kim I., et al., Synthesis and properties of the conjugated polymers with indenoindene and benzimidazole units for organic photovoltaics. J. Polym. Sci. A1, 2013, 51, 241-249.
26. Xiang G., Lin S., Cui W., Wang L., Zhou L., Li L., et al., Metal complex of polymer with 2-(pyridin-2-yl)-1H-benzo[d]imidazole unit as a selectivity-tunable chemosensor for amino acids. Sensor. Actuat. B-Chem., 2013, 188, 540-547.
27. Xiang G., Cui W., Lin S., Wang L., Meier H., Li L., et al., A conjugated polymer with ethyl 2-(2-(pyridin-2-yl)-1H-benzo[d] imidazol-1-yl) acetate units as a novel fluorescent chemosensor for silver(I) detection. Sensor. Actuat. B-Chem., 2013, 186, 741-749.
28. Kou C., He X., Jiang X., Ni Y., Liu L., Huangfu C., et al., Novel isoindigo-based conjugated polyelectrolytes: Synthesis and fluorescence quenching behavior with water-soluble poly(p-phenylenevinylene)s. J. Polym. Sci. A1, 2015, 53, 2223-2237.
29. Gershon H., Clarke D.D., Gershon M., Preparation and Fungitoxieity of 3,6-Diehloroand 3,6-Dibromo-8-Quinolinols. Monatsh. Chem., 1994, 125, 723-730.
30. Wilson J.G., Hunt F.C., Iminodiacetic acid derivatives of benzimidazole. Synthesis of N-(Benzimidazol-2-ylmethyl) iminodiacetic acids. Aust. J. Chem., 1983, 36, 2317.
31. Cheng Y.-J., Luh T.-Y., Synthesizing optoelectronic heteroaromatic conjugated polymers by cross-coupling reactions. J. Organomet. Chem., 2004, 689, 4137-4148.
32. Willis-Fox N., Gutacker A., Browne M.P., Khan A.R., Lyons M.E.G., Scherf U., et al., Selective recognition of biologically important anions using a diblock polyfluorene–polythiophene conjugated polyelectrolyte. Polym. Chem.-UK, 2017, 8, 7151-7159.
33. Schanze K., Pinto M., Conjugated Polyelectrolytes: Synthesis and Applications. Synthesis, 2002, 2002, 1293-1309.
34. Tan C., Atas E., Muller J.G., Pinto M.R., Kleiman V.D., Schanze K.S., Amplified quenching of a conjugated polyelectrolyte by cyanine dyes. J. Am. Chem. Soc., 2004, 126, 13685-13694.
35. Shen H., Kou C., He M., Yang H., Liu K., Synthesis and surfactochromicity of 1,4-diketopyrrolo[3,4-c]pyrrole(DPP)-based

anionic conjugated polyelectrolytes. J. Polym. Sci. A1, 2014, 52, 739-751.
36. Liu K., Li Y., Yang M., Synthesis and solution properties of a meta-linked anionic poly(phenylene ethynylene) conjugated polyelectrolyte. e-Polymers, 2012, 12, 1-8.
37. Tan C., Pinto M.R., Schanze K.S., Photophysics, aggregation and amplified quenching of a water-soluble poly(phenylene ethynylene). Chem. Commun., 2002, 446-447.
38. Crosby G.A., Demas J.N., Measurement of photoluminescence quantum yields. Review. J. Phys. Chem., 1971, 75, 991-1024.
39. Fan Q.-L., Zhang G.-W., Lu X.-M., Chen Y., Huang Y.-Q., Zhou Y., et al., Cationic phenyl-substituted poly(p-phenylenevinylene) related copolymers with efficient photoluminescence and synthetically tunable emissive colors. Polymer, 2005, 46, 11165-11173.
40. Treger J.S., Ma V.Y., Gao Y., Wang C.C., Wang H.L., Johal M.S., Tuning the optical properties of a water-soluble cationic poly(p-phenylenevinylene): surfactant complexation with a conjugated polyelectrolyte. J. Phys. Chem. B, 2008, 112, 760-763.
41. Long Y., Chen H., Wang H., Peng Z., Yang,Y., Zhang G., et al., Highly sensitive detection of nitroaromatic explosives using an electrospun nanofibrous sensor based on a novel fluorescent conjugated polymer. Anal. Chim. Acta, 2012, 744, 82-91.
42. Ceniceros-Gomez A.E., Ramos-Organillo A., Hernandez-Diaz J., Nieto-Martinez J., Contreras R., Castillo-Blum S.E., NMR study of the coordinating behavior of 2,6-bis(Benzimidazol-2'-yl) pyridine. Heteroatom Chem., 2000, 11, 392-398.
43. Zhang Y., Wang G., Zhang J., Study on a highly selective fluorescent chemosensor for Fe^{3+} based on 1,3,4-oxadiazole and phosphonic acid. Sensor. Actuat. B-Chem., 2014, 200, 259-268.
44. Dhara A., Jana A., Guchhait N., Ghosh P., Kar S.K., Rhodamine-based molecular clips for highly selective recognition of Al^{3+} ions: synthesis, crystal structure and spectroscopic properties. New J. Chem., 2014, 38, 1627-1634.